



1 **Impacts of South Asian aerosol inflow over Mount Qomolangma**
2 **on downstream cloud–precipitation processes through a long–**
3 **range ice-crystal “seeding” effect**

4
5 Xiangde Xu^{1, a}, Wenyue Cai^{1, a}, Tianliang Zhao², Changjun Yang³, Kai Meng⁴, Chong Wu¹, Na Dong^{1, 5},
6 Yueqing Li⁶, Shunjiu Wang⁶, Wenqing Liu⁷, Tianshu Zhang⁷, Ga Zhuo⁸, Shengjun Zhang¹, Bin Chen¹,
7 Chunsong Lu², Jinghua Chen², Kai Yang², Jianming Xu⁹

8
9 ¹ State Key Laboratory of Severe Weather Meteorological Science and Technology, Chinese Academy of
10 Meteorological Sciences, Beijing 100081, China

11 ² Key Laboratory for Aerosol-Cloud-Precipitation of China Meteorological Administration, Nanjing
12 University of Information Science and Technology, Nanjing, Jiangsu Province, 210044, China

13 ³ Key Laboratory of Radiometric Calibration and Validation for Environmental Satellites, National
14 Satellite Meteorological Center (National Centre for Space Weather), China Meteorological
15 Administration, Beijing 100081, China

16 ⁴ Hebei Key Laboratory of Meteorology and Modern Economy, Hebei Provincial Institute of
17 Meteorological Sciences, Shijiazhuang 050021, China

18 ⁵ Department of Atmospheric and Oceanic Sciences & Institute of Atmospheric Sciences, Fudan
19 University, Shanghai, 200438, China

20 ⁶ Heavy Rain and Drought-Flood Disaster in Plateau and Basin Key Laboratory of Sichuan Province,
21 Chengdu Institute of Plateau Meteorology, China Meteorological Administration, Chengdu 610072, China

22 ⁷ Key Laboratory of Environment Optics and Technology, Anhui Institute of Optics and Fine Mechanics,
23 Chinese Academy of Sciences, Hefei 230031, China

24 ⁸ Mêdog National Climate Observatory, Mêdog, 860700, China

25 ⁹ Shanghai Meteorological Center, Shanghai Meteorological Service, Shanghai 200030, China



26

27 ^a These authors contributed equally to this work as co-first authors.

28 Corresponding authors: Wenyue Cai (caiwy@cma.gov.cn), TianLiang Zhao (tlzhao@nuist.edu.cn)

29

30 **Abstract.** Mount Qomolangma (MQ) serves as a natural laboratory for investigating aerosol–
31 cloud–precipitation interactions over the Tibetan Plateau (TP). Using satellite and
32 comprehensive ground-based observations, we identify pronounced ice-cloud activation
33 associated with transported exogenous aerosols. Under different large-scale atmospheric
34 circulation regimes, ice-phase cloud activated over MQ can be efficiently transported
35 downstream through distinct pathways, exerting a pronounced ice crystal seeding effect on
36 cloud–precipitation conversion. The spatial patterns of these downstream pathways are highly
37 consistent with regions of enhanced ice-phase occurrence, precipitation, and upper-
38 tropospheric latent heat release. This study provides new insight into the downstream impacts
39 of aerosol transport through ice seeding for cloud precipitation. The findings highlight the
40 important role of aerosol-induced ice-phase processes in modulating cloud and precipitation
41 systems over the “Third Pole” and its downstream regions, with significant implications for
42 understanding downstream extreme precipitation and environment change under South Asian
43 increasing anthropogenic influences.

44 **Keywords:** aerosol–cloud–precipitation interactions, ice-cloud activation, ice crystal seeding
45 effect, the downstream impacts of aerosol transport, Mount Qomolangma

46

47 **1 Introduction**

48 The evolution of precipitation is complex and occurs in various forms, influenced not only by multiple physical
49 processes—such as vertical motion within clouds, liquid water production, turbulent structures, and cloud
50 lifetimes—but also by the characteristics of aerosol loading (Twomey et al., 1984; Levin and Cotton 2009; Xu et
51 al., 2025). Theoretically, aerosols exert the significant influence on both the development of clouds and the
52 formation of precipitation from the macrophysical and microphysical perspectives (Zhang et al., 2017; Zhou et
53 al., 2017; Zhao et al., 2024). Aerosols can act as cloud condensation nuclei (CCN) or ice nuclei (IN), altering



54 cloud microphysical properties and precipitation processes (Twomey, 1977; Penner et al., 2001; Rosenfeld et al.,
55 2014; Zhao et al., 2025). However, for a long time, the role of anthropogenic aerosols in modulating rainfall has
56 long remained a contentious issue in climate science, with substantial evidence supporting both enhancement
57 (Khain et al., 2005; Fan et al., 2018) and suppression (Qian et al., 2009; Liu et al., 2011; Guo et al., 2016; Liu et
58 al., 2020b) effects. Regional studies further emphasize such complexity (Giorgi et al., 2002; Menon et al., 2002).

59 Mounting evidence suggests that the southern slopes of the Himalayas now serve as a major transport
60 pathway and sensitive receptor zone for aerosols originating from South Asia (Hindman and Upadhyay, 2002;
61 Ramanathan et al., 2005; Huang et al., 2007; Lawrence, 2011; Ming et al., 2013; Liu et al., 2015; Cong et al.,
62 2015; Kang et al., 2019; Li et al., 2020; Liu et al., 2020a; Wang et al., 2020; Zhao et al., 2020). This implies that
63 an issue of aerosols influencing cloud properties have emerged as a new challenge for research on the role of the
64 Tibetan Plateau (TP) in climate change. Xu et al. (2025) found that during the Indian summer monsoon, aerosols
65 from South Asia have a distinct activation effect on the cloud-precipitation process over the Mount Qomolangma
66 (MQ). Under dynamic lifting, the increase in aerosols, which inhibits and delays weak precipitation over the MQ,
67 instead intensifies the development of clouds over the MQ, leading to heavy precipitation on the north slope. The
68 synergy of the MQ thermal-dynamic driving mechanism and the aerosol activation effect can trigger the deep
69 convection in the precipitation process on the north slope of the MQ. Cloud development is more intense with the
70 aerosol activation effect. MQ serves as a natural laboratory for investigating aerosol–cloud–precipitation
71 interactions over the TP. Despite these impacts, the intricate interactions between aerosol and cloud microphysics
72 make the effects of aerosol on precipitation poorly understood (Levin and Cotton 2009; IPCC Climate Change
73 2013), and understanding of aerosol–cloud–precipitation interactions over the TP and their downstream impacts
74 remains particularly limited.

75 Meanwhile, as the roof of the world, the TP acts as a vast engine, driving the nearby movements of water
76 vapor, clouds, and aerosols (Kang et al., 2019; Liu et al., 2020a). The TP shows prominent transport characteristics
77 of cloud systems and water vapor over itself and surrounding regions. Such eastward transport effect is vital to
78 the formation of precipitation processes and even floods in downstream eastern China. (Xu et al., 2001, 2002,
79 2006; Miao et al., 2002; Zhuo et al., 2002; Wan et al., 2017). Nevertheless, previous studies have only examined
80 the effects of aerosols over the TP and its surrounding areas on local precipitation (Jiang et al., 2023; Ying et al.,
81 2023). without considering the possible upstream-downstream linkage effects between the plateau and eastern
82 China induced by the transport effect of the TP.

83 As part of the Second Tibetan Plateau Scientific Expedition and Research Program (STEP), a comprehensive



84 vertical observation experiment focusing on aerosol–cloud–precipitation interactions was carried out in the MQ
85 region (Xu et al., 2025). This observational framework combines ground-based aerosol lidar measurements, X-
86 band dual-polarization weather radar observations for mesoscale weather systems, routine surface meteorological
87 observations and satellite observations (Ma et al., 2023; Xu et al., 2025). Leveraging these coordinated
88 measurements, we herein explore the impacts of South Asian aerosol inflow over MQ on downstream cloud-
89 precipitation processes. In particular, the activation of ice-phase clouds by transported aerosols and the subsequent
90 long-range downstream transport of ice nuclei may exert a “seeding” effect, whereby ice crystals enhance cloud-
91 precipitation conversion processes far from their source regions. Such mechanisms could alter latent heat release,
92 cloud dynamics, and precipitation patterns in downstream areas of East Asia. Consequently, investigating the
93 pathways and mechanisms through which aerosol-activated ice clouds influence downstream cloud–precipitation
94 systems holds fundamental scientific significance and practical relevance in the context of climate change and
95 increasing anthropogenic activities.

96

97 **2 Data and methods**

98 **2.1 Aerosol lidar observations**

99 A ground-based lidar system manufactured by the Anhui Institute of Optics and Fine Mechanics, Chinese
100 Academy of Sciences, was deployed at the MQ site to conduct continuous observations of aerosol extinction
101 coefficients (AEC) during July 2018 and July 2019 (Xiang et al., 2021; Ma et al., 2023). The AEC was retrieved
102 using the Fernald inversion method (Fernald, 1984), and cloud contamination was removed using an empirical
103 threshold-based cloud-screening algorithm (Liu and Sugimoto, 2002). Detailed quality-control procedures follow
104 those described by Xiang et al. (2020). In this study, aerosol conditions were classified based on daily mean AEC
105 values at the MQ site (Xu et al., 2025). Days with $AEC \geq 0.025 \text{ km}^{-1}$ were defined as high-aerosol-loading events,
106 whereas days with $AEC < 0.025 \text{ km}^{-1}$ were classified as low-aerosol-loading events for both July 2018 and July
107 2019 (Table S1).

108 **2.2 X-band dual-polarization radar observations**

109 An X-band dual-polarization weather radar, provided by the Institute of Plateau Meteorology, China



110 Meteorological Administration, Chengdu, was operated at the MQ site during July 2019 (Ma et al., 2023). The
111 radar data underwent comprehensive quality-control procedures, including ground-clutter suppression, noise-bias
112 correction of correlation coefficients and differential reflectivity, differential phase filtering, estimation of
113 differential propagation phase shift, and attenuation correction for reflectivity and differential reflectivity (Xiao
114 et al., 2012; Wang et al., 2019). These processed radar observations were used to characterize convective intensity
115 and precipitation-related microphysical features and to examine their relationships with aerosol loading and cloud-
116 phase variations.

117 **2.3 Satellite cloud-phase products**

118 Hourly full-disk cloud-phase products from the FengYun-4A Advanced Geosynchronous Radiation Imager (FY-
119 4A/AGRI), provided by the National Satellite Meteorological Center of China, were used to identify cloud-phase
120 distributions. The data are provided in a nominal projection with a spatial resolution of 4 km at nadir. Cloud-phase
121 statistics for July 2018 and July 2019 were derived to examine the upstream–downstream relationships between
122 aerosol loading, cloud-phase occurrence, and precipitation under high- and low-aerosol conditions at the MQ site.

123 **2.4 Aerosol optical depth data**

124 Monthly aerosol optical depth (AOD) data at 0.55 micron from the MODIS Combined Dark Target and Deep Blue
125 Collection 6.1 product were used to characterize long-term aerosol distribution and trends over South Asia and
126 East Asia during July 2000–2020. The data have a spatial resolution of $1^\circ \times 1^\circ$, which is particularly suitable for
127 bright surfaces such as plateaus, deserts, and arid regions (Levy et al., 2013; Sayer et al., 2014; de Leeuw et al.,
128 2018).

129 **2.5 Meteorological observations and reanalysis data**

130 Hourly and daily surface meteorological observations were obtained from the Data Sets of Surface Meteorological
131 Elements in China released by the National Meteorology Information Center, China Meteorological
132 Administration. These data were used to analyze precipitation variability and its relationship with aerosol and
133 cloud-phase anomalies in downstream regions.

134 To examine large-scale circulation patterns and latent heat distributions associated with different aerosol-
135 loading conditions, hourly and monthly meteorological reanalysis data for July 2018 and July 2019 were obtained



136 from the European Centre for Medium-Range Weather Forecasts. The data have a horizontal resolution of 0.25°
137 $\times 0.25^\circ$ and were used to characterize atmospheric circulation structures and thermodynamic anomalies linked to
138 aerosol-induced cloud and precipitation responses.

139

140 **3 Results**

141 **3.1 Aerosol–cloud phase relationships in deep convective systems over the MQ**

142 Recently, the spatial correlation of the daily AOD with cloud properties and precipitation during both wet and dry
143 monsoonal years indicated a positive association of relatively high aerosol concentrations with cloud vertical
144 development and precipitation (Adhikari and Mejia, 2021). Satellite observations indicate pronounced aerosol
145 optical depth (AOD) over South Asia and the Himalayan region, with a zonally elongated band of high correlation
146 between South Asian aerosols and aerosol loading along the southern TP margin near MQ (Fig. 1a). This high-
147 AOD belt, stretching from the South Asian plains to the Himalayan foothills, is commonly known as the
148 Atmospheric Brown Cloud (Ramanathan et al., 2005; Zhao et al., 2020). Interannual variability in July AOD from
149 2000 to 2020 further reveals persistent and intensifying aerosol accumulation along the southern Himalayan slopes,
150 originating from South Asia and showing a clear upward trend (Fig. 1b). These aerosols have been demonstrated
151 to substantially influence cloud microphysical processes and precipitation patterns (Xu et al., 2025).

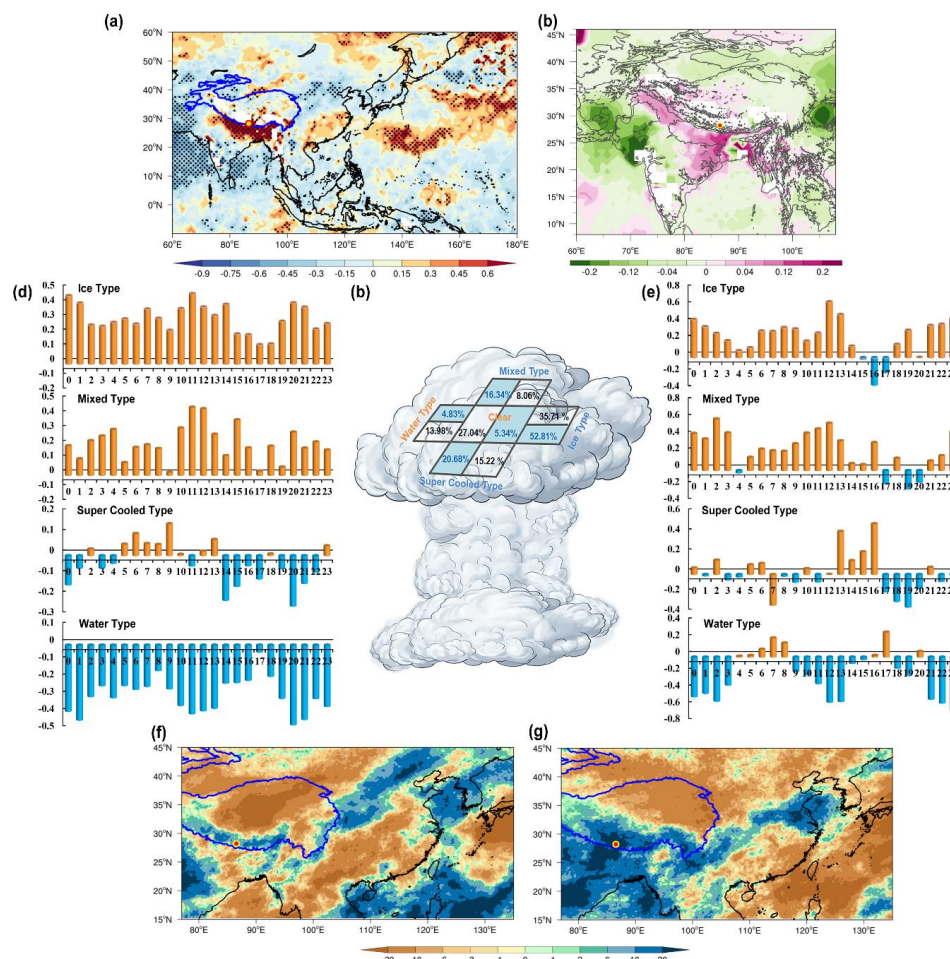
152 Relatively, the aerosol loading over the TP is much lower than those over other regions, thus leading to the
153 more sensitive response of precipitation to aerosol-cloud interactions (Liu et al., 2022). Cloud and precipitation
154 processes are easily affected in relatively clean atmospheric environments (Garrett and Zhao, 2006; Zhao et al.,
155 2020). Previous studies have already revealed that absorbing aerosols over the TP have been proposed to directly
156 affect monsoon rainfall through the elevated-heat-pump mechanism (Lau et al., 2008; Luo et al., 2020; Liu et al.,
157 2022). During the Indian summer monsoon, low-level moist air masses originating from the Arabian Sea transport
158 substantial aerosol loads across the Indian subcontinent and ascend along the southern slopes of the Himalayas
159 toward MQ, supplying abundant CCN and IN essential for orographic cold-cloud precipitation. Observations
160 reveal a positive correlation between aerosol concentration and the abundance of ice-phase hydrometeors in anvil
161 clouds; the associated latent heat release from enhanced freezing further intensifies updrafts. Satellite-derived
162 cloud-phase statistics demonstrate that under high aerosol loading, the occurrence frequencies of ice-phase,
163 supercooled liquid, and mixed-phase clouds are 52.81%, 20.68%, and 16.34%, respectively—compared to 35.71%,



164 15.22%, and 8.06% under low aerosol loading. Conversely, liquid-phase clouds occur significantly more
165 frequently under low aerosol conditions (13.98%) than under high aerosol conditions (4.83%) (Fig. 1c). Compared
166 with water clouds, ice clouds are observed more frequently and are more significantly correlated with aerosols
167 over the TP, which is consistent with prior observational and modeling evidence (Hua et al., 2020).

168 An integrated analysis of the diurnal cycles of aerosol extinction coefficients from lidar observations,
169 maximum radar reflectivity from X-band dual-polarization radar, and cloud-phase frequencies further reveals that
170 aerosol concentrations exhibit a statistically robust positive correlation exclusively with ice-phase and mixed-
171 phase cloud occurrences—not with liquid- or supercooled liquid-phase clouds (Fig. 1d, 1e). Moreover, ice-phase
172 and mixed-phase clouds display in-phase peak–trough relationships with the diurnal cycle of maximum radar
173 reflectivity (Fig. 1d, 1e), indicating that these cloud types represent the dominant manifestation of aerosol-induced
174 deep convective activation. Aerosol concentrations significantly promote the formation of ice-phase and mixed-
175 phase clouds in deep convective systems, whereas low aerosol concentrations favor the persistence of liquid-phase
176 clouds. Under the combined effects of strong orographic lifting and enhanced thermodynamic forcing over MQ,
177 aerosol-induced apparent heat sources facilitate the formation of additional ice clouds. The associated latent heat
178 release enables more numerous and smaller cloud droplets to be lifted to higher altitudes, enhancing collision,
179 riming, and aggregation processes among ice crystals and cloud droplets. High concentrations of carbonaceous
180 aerosols, acting as efficient ice nuclei, preferentially activate convective clouds dominated by ice-phase and
181 mixed-phase hydrometeors, thereby intensifying deep convection over MQ. This finding aligns with prior
182 observational and modeling evidence showing that high aerosol loading enhances deep convective cloud
183 invigoration and strengthens the apparent heat source over MQ (Xu et al., 2025), thereby may further intensifying
184 thermodynamic forcing on downstream cloud and precipitation systems.

185



186
 187 **Figure 1.** Aerosol distribution and cloud-phase responses over MQ: (a) Spatial correlation between AOD
 188 over the MQ region and East Asia during July 2000–2020, dotted regions indicate correlations statistically
 189 significant at the 90% confidence level ($P > 0.1$, $n = 21$); (b) Linear trends of July AOD over South Asia and
 190 the Himalayan region during 2000–2020; (c) Percentage contributions of ice-phase, mixed-phase,
 191 supercooled liquid, and liquid clouds under high- versus low-aerosol-loading conditions during July 2018
 192 and July 2019; (d) Diurnal variation in the correlation coefficient between lidar-derived aerosol extinction
 193 coefficient and cloud-phase occurrence ($n = 62$, July 2018 and July 2019); (e) Diurnal variation in the
 194 correlation coefficient between maximum radar reflectivity from X-band dual-polarization radar and cloud-
 195 phase occurrence ($n = 31$, July 2019); (f, g) Spatial distributions of daily ice-phase cloud-frequency
 196 anomalies under high versus low aerosol loading for (f) July 2018 and (g) July 2019.

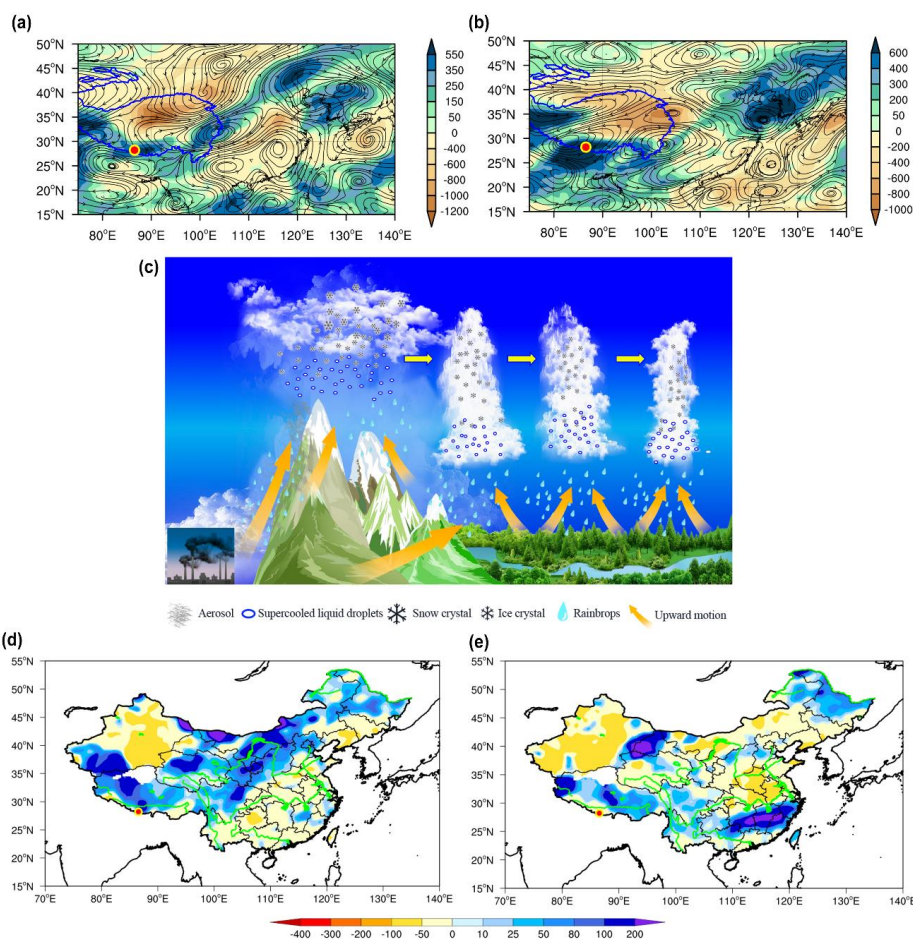


197

198 **3.2 Downstream transport pathways and cloud–precipitation responses**

199 The TP dynamically operates as a quasi-stationary large-scale vortex, facilitating the transport of moisture, clouds,
200 and aerosols from lower latitudes to higher elevations (Xu et al., 1998, 2001, 2002, 2006; Zhuo et al., 2002; Wan
201 et al., 2017; Kang et al., 2019; Liu et al., 2020a). Then, aerosol–cloud interactions over the TP may not only affect
202 the local precipitation but also contribute to downstream precipitation. Variations in large-scale circulation
203 patterns modulate the upstream–downstream impacts of high versus low aerosol loading, giving rise to distinct
204 downstream pathways of cloud-phase anomalies (Fig. S1). Compared with low aerosol conditions, high aerosol
205 loading over MQ leads to notably stronger cloud–precipitation activation and more pronounced downstream
206 effects. In particular, downstream anomalies are dominated by ice-phase and mixed-phase clouds, rather than
207 liquid or supercooled liquid clouds. In July 2018, the downstream pathway of ice-phase and mixed-phase cloud-
208 frequency anomalies associated with high aerosol loading extended from MQ along a southwest–northeast
209 corridor toward the northeastern Tibetan Plateau and the Yellow River basin. In contrast, during July 2019, the
210 anomaly pathway extended predominantly eastward from MQ along the Yangtze River and Huai River basins.
211 Figure 1f and 1g illustrate the banded upstream–downstream distributions of daily ice-phase and mixed-phase
212 cloud-frequency anomalies under high versus low aerosol conditions for July 2018 and July 2019, respectively.

213



214

215 **Figure 2.** Downstream pathways of latent heat release and precipitation anomalies: (a, b) Anomalies in 300-
 216 hPa atmospheric circulation (first-order filtered) and latent heat release under high- versus low-aerosol-
 217 loading conditions over MQ for (a) July 2018 and (b) July 2019; (c) Conceptual schematic illustrating the
 218 ice-nucleating role of externally transported aerosols in promoting ice-cloud-precipitation conversion and
 219 modulating downstream precipitation; (d, e) Spatial distributions of precipitation anomalies associated with
 220 high- versus low-aerosol-loading conditions for (d) July 2018 and (e) July 2019.

221

222 When numerous ice crystals form through vapor sublimation and the freezing of lofted cloud droplets,
 223 substantial latent heat is released, further intensifying convective development (Rosenfeld, 2006). Analysis of
 224 300-hPa circulation anomalies and latent heat release anomalies under high- versus low-aerosol-loading
 225 conditions over MQ for July 2018 and 2019 reveals that the spatial distribution of latent heat anomalies (Fig. 2a,



226 [2b](#)) align closely with that of the pathways of ice-phase and mixed-phase cloud-frequency anomalies ([Fig. 1f, 1g](#)),
227 as well as the corresponding precipitation anomalies ([Fig. 2d, 2e](#)). [Figure 2d and 2e](#) illustrate that precipitation
228 anomalies associated with high versus low aerosol loading over MQ also exhibit distinct downstream pathways.
229 In July 2018, precipitation anomalies form a southwest–northeast-oriented band extending toward the northeastern
230 TP and the Yellow River basin, while in July 2019, the anomalies extend eastward along the Yangtze and Huai
231 River basins. This reveals that high aerosol loading over MQ exerts a dual influence along downstream transport
232 pathways: it enhances cloud ice–precipitation conversion through effective glaciation seeding, and it induces
233 pronounced banded anomalies in upper-tropospheric latent heat release. Among these, ice-nucleating particles
234 (INPs) initiate heterogeneous ice nucleation in supercooled clouds ([Lohmann and Feichter, 2005](#)). Aerosol-
235 enhanced deep convection over MQ propagates thermodynamic perturbations over long distances, driving
236 coordinated ice-cloud development, cloud–ice interactions, and vertically distributed latent heat release across
237 multiple tropospheric layers. Through this cascade, ice crystals serve as precipitation embryos that seed lower-
238 level clouds and reorganize precipitation spatial patterns along climatically sensitive downstream corridors,
239 ultimately reshaping regional cloud regimes and precipitation distributions over Eastern China ([Fig. 2c](#)).

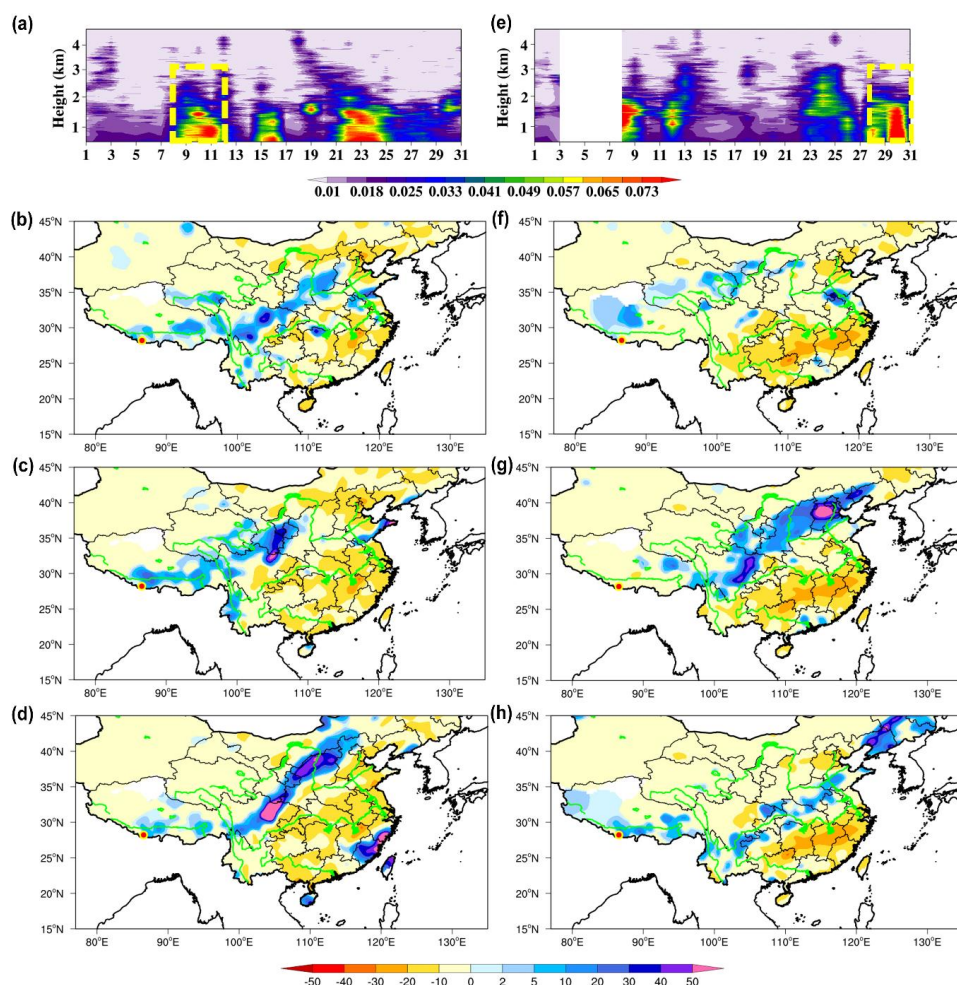
240

241 **3.3 Seeding effects of aerosol-activated ice clouds on downstream precipitation**

242 To further confirm the seeding effects of aerosol-activated ice clouds on downstream precipitation, we perform
243 tracking analyses of upstream high-aerosol events to investigate their influences on downstream precipitation in
244 the following three days, that is, the downstream precipitation-affected regions evolve continuously starting from
245 the pollution day over the subsequent two days. As shown in [Figure 3](#), with the occurrence of upstream high-
246 aerosol episodes, intense precipitation gradually develops over eastern downstream regions, and higher
247 precipitation is observed. These heavy precipitation belts align closely with the high-frequency downstream
248 pathways of ice-phase and mixed-phase clouds linked to high aerosol loading ([Fig. 1f, 1g](#)), as well as the spatial
249 distribution of latent heat anomalies ([Fig. 2a, 2b](#)). This further confirms the seeding effects of aerosol-activated
250 ice clouds on downstream precipitation. From a physical perspective, one important mechanism within mid-
251 latitude stratiform and mixed-phase cloud precipitation systems is the seeder-feeder mechanism, known to
252 significantly enhance precipitation and thus play a critical role in the Earth's water cycle ([Purdy et al., 2005](#); [He
253 et al., 2015](#); [Heymsfield et al., 2020](#)). Seeder clouds, which can be pure ice or mixed-phase clouds themselves,



254 produce ice crystals, for example supported by INPs, that fall into feeder clouds below (Ramelli et al., 2021).
255 Feeder clouds, acting as a moisture reservoir, typically mainly consist of supercooled liquid cloud droplets that
256 contribute to the growth of falling ice crystals or to an enhancement of particle number and ice mass (Hosler et
257 al., 1957). The Wegener-Bergeron-Findeisen process (Wegener, 1911; Bergeron, 1935; Findeisen, 1938), where
258 water vapor preferentially deposits onto ice crystals at the expense of supercooled droplets, accelerates ice growth
259 and enhances precipitation. In this framework, upper-level ice crystals serve as precipitation embryos, while the
260 abundant supercooled liquid water in the lower cloud layers provides the essential microphysical environment for
261 their growth into precipitating hydrometeors. Furthermore, the contrasting downstream precipitation pathways
262 between the two years underscore the critical role of background circulation patterns—such as the subtropical
263 high and monsoon system configurations—in shaping aerosol-induced cloud–precipitation responses.
264



265

266 **Figure 3.** Temporal evolution of downstream precipitation responses: (a, e) Daily variations in AEC over
 267 MQ during (a) July 2018 and (e) July 2019 (Xu et al., 2025); yellow boxes denote selected high-aerosol
 268 events (9–11 July 2018; 28–30 July 2019). (b–d, f–h) Composite precipitation anomalies downstream on (b,
 269 f) the pollution day, (c, g) the second day, and (d, h) the third day following high-aerosol events for (b–d)
 270 July 2018 and (f–h) July 2019.

271

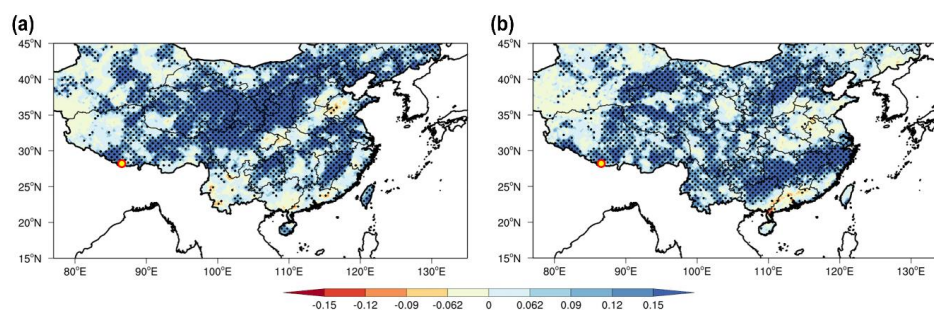
272 Based on satellite-derived cloud-phase data and ground-based aerosol lidar observations, we further quantify
 273 the relative contributions of different cloud phases under high and low aerosol conditions. Given that ice-phase
 274 clouds show the most pronounced enhancement under high aerosol loading (Fig. S1), we analyze the relationship
 275 between daily ice-phase cloud frequency and daily precipitation in the eastern TP downstream regions during July



276 2018 and July 2019. [Figure 4a and 4b](#) indicate that the identified high-impact downstream pathways correspond
277 to regions with a strong positive correlation between ice-phase cloud occurrence and precipitation. Furthermore,
278 the spatial patterns of positive precipitation and ice-phase cloud anomalies are broadly consistent across both
279 months.

280 These findings provide additional evidence that high concentrations of transported aerosols over MQ
281 enhance deep convective cloud development and facilitate the downstream transport of upper-level ice clouds,
282 which can act as effective seeding agents to intensify cloud–precipitation cycling. This mechanism implies that
283 increasing anthropogenic aerosol emissions in South Asia may not only activate deep convection over the southern
284 TP but also modulate precipitation patterns in downstream regions.

285



286

287 **Figure 4.** Relationship between ice-phase cloud occurrence and precipitation: (a, b) Spatial distributions of
288 the Pearson correlation coefficient between ice-phase cloud frequency and hourly precipitation for (a) July
289 2018 and (b) July 2019; dotted regions indicate correlations statistically significant at the 95% confidence
290 level ($P > 0.05$, $n = 744$).

291

292 **4 Conclusion**

293 Using synergistic observation data from the STEP comprehensive vertical observation experiment concerning
294 aerosol–cloud–precipitation interactions over MQ, to explore the impacts of South Asian aerosol inflow over MQ
295 on downstream cloud–precipitation processes. The findings reveal that MQ exhibits high sensitivity to externally
296 transported, high-concentration aerosols, which preferentially enhance ice-phase cloud formation and invigorate
297 deep convective precipitation. The enhanced formation of ice-phase clouds leads to increased latent heat release,



298 intensifying thermodynamic forcing over the TP and altering large-scale circulation patterns. Through long-range
299 transport, aerosol-activated ice crystals are conveyed downstream, establishing a distinct “seeder–feeder”–type
300 ice–cloud–precipitation conversion mechanism between upper- and lower-level clouds. A key discovery is that the
301 upstream–downstream transmission is achieved via the long-range ice-crystal “seeding” effect. This process
302 generates coherent downstream pathways characterized by enhanced ice-phase cloud occurrence, latent heat
303 anomalies, and precipitation responses.

304 The identified downstream pathways vary interannually, reflecting differences in background circulation
305 associated with the monsoon system and the subtropical high. These results reveal a previously underappreciated
306 role of long-range aerosol transport in modulating cloud–precipitation coupling over the “Third Pole” and its
307 downstream regions, and demonstrate that aerosols play a dual role in shaping precipitation patterns across the TP
308 and China while exerting adverse impacts on human living environments. Enhanced South Asian aerosol transport
309 may increase the likelihood of extreme rainfall events in downstream regions and contribute to uneven flood–
310 drought conditions.

311 Taken together, these findings provide new physical insights into how increasing anthropogenic aerosols
312 under climate change may influence regional precipitation patterns and hydrological processes across East Asia.
313 They further suggest a potentially important, yet still insufficiently quantified, pathway through which enhanced
314 South Asian aerosol transport may affect downstream extreme precipitation and environment change via aerosol-
315 induced ice-phase cloud processes. Future work will explore and expand upon its quantitative mechanisms.

316

317 **Code availability.** The code developed for this study is available from the corresponding
318 author on reasonable request.

319



320 **Data availability.** The continuous Lidar and X-band dual-polarization weather radar
321 observation data used in this study were authorized and provided by the Anhui Institute of
322 Optics and Fine Mechanics of Chinese Academy of Sciences and Chengdu Institute of Plateau
323 Meteorology of China Meteorological Administration, respectively. Access to these datasets
324 requires formal request submission to the corresponding author upon adherence to institutional
325 data-sharing protocols regulating data usage. The hourly cloud phase full disk product of FY-
326 4A/Advanced Geosynchronous Radiation Imager (AGRI) is provided by the National Satellite
327 Meteorological Center., which can be found at
328 <https://data.nsmc.org.cn/DataPortal/cn/data/dataset.html>. Monthly aerosol optical depth (AOD)
329 data at 550 nm from the MODIS Collection 6.1 product which can be found at
330 <https://giovanni.gsfc.nasa.gov/giovanni/>. Observation data of common meteorological
331 elements used in this study are derived from the Data Sets of Surface Meteorological Elements
332 in China released by the National Meteorology Information Center, China Meteorological
333 Administration, which can be found at <http://cdc.cma.gov.cn>. ERA5 is the fifth generation
334 ECMWF reanalysis for the global climate and weather, which can be found at
335 [https://cds.climate.copernicus.eu/datasets/reanalysis-era5-pressure-levels-monthly-](https://cds.climate.copernicus.eu/datasets/reanalysis-era5-pressure-levels-monthly-means?tab=overview)
336 [means?tab=overview](https://cds.climate.copernicus.eu/datasets/reanalysis-era5-pressure-levels?tab=overview) and [https://cds.climate.copernicus.eu/datasets/reanalysis-era5-pressure-](https://cds.climate.copernicus.eu/datasets/reanalysis-era5-pressure-levels?tab=overview)
337 [levels?tab=overview](https://cds.climate.copernicus.eu/datasets/reanalysis-era5-pressure-levels?tab=overview).

338



339 **Author contributions.** All the authors made contributions to this research and manuscript. XX
340 and WC contributed equally to this research. XX, WC and TZ conceived and designed the
341 project. CY, CW, KM, TZ, YL and SW collected the data. WC processed data and prepared
342 most figures. ND prepared Figure 3a and 3b. XX, WC and TZ analysed the study results and
343 drafted the manuscript. All authors participated in scientific discussions, revised the manuscript,
344 and approved the final version for publication.

345

346 **Competing interests.** The contact author has declared that none of the authors has any
347 competing interests.

348

349 **Acknowledgements.** This study was supported by the Second Tibetan Plateau Scientific
350 Expedition and Research Program (STEP, grant no. 2019QZKK0105), Major Science and
351 Technology Project of Tibet Autonomous Region (grant no. XZ202402ZD0006-06) and the
352 National Natural Science Foundation of China (grant no. U2242208). We deeply appreciate the
353 National Observation and Research Station of China for Qomolangma Special Atmospheric
354 Processes and Environmental Changes providing data support for this study.

355 **Financial support.** This research has been supported by the Second Tibetan Plateau Scientific
356 Expedition and Research Program (STEP, grant no. 2019QZKK0105), Major Science and
357 Technology Project of Tibet Autonomous Region (grant no. XZ202402ZD0006-06) and the
358 National Natural Science Foundation of China (grant no. U2242208).

359

360 **References**

361 Adhikari, P. and Mejia, J. F.: Influence of aerosols on clouds, precipitation and freezing level
362 height over the foothills of the Himalayas during the Indian summer monsoon, *Clim. Dyn.*,



- 363 57, 395–413, <https://doi.org/10.1007/s00382-021-05710-2>, 2021.
- 364 Bergeron, T.: On the physics of cloud and precipitation, in: Proceedings of the Fifth Assembly
365 of the International Union of Geodesy and Geophysics, Lisbon, Portugal, IUGG, 156–178,
366 1935.
- 367 Cong, Z. Y., Kawamura, K., Kang, S. C., and Fu, P. Q.: Penetration of biomass-burning
368 emissions from South Asia through the Himalayas: new insights from atmospheric organic
369 acids, *Sci. Rep.*, 5, 9580, <https://doi.org/10.1038/srep09580>, 2015.
- 370 de Leeuw, G., Sogacheva, L., Rodriguez, E., Kourtidis, K., Georgoulas, A. K., Alexandri, G.,
371 Amiridis, V., Proestakis, E., Marinou, E., Xue, Y., and van der A, R.: Two decades of satellite
372 observations of AOD over mainland China using ATSR-2, AATSR and MODIS/Terra: data
373 set evaluation and large-scale patterns, *Atmos. Chem. Phys.*, 18, 1573–1592,
374 <https://doi.org/10.5194/acp-18-1573-2018>, 2018.
- 375 Fan, J. W., Rosenfeld, D., Zhang, Y. W., Giangrande, S. E., Li, Z. Q., Machado, L. A. T., Martin,
376 S. T., Yang, Y., Wang, J., Artaxo, P., Barbosa, H. M. J., Braga, R. C., Comstock, J. M., Feng,
377 Z., Gao, W. H., Gomes, H. B., Mei, F., Pöhlker, C., Pöhlker, M. L., Pöschl, U., and de Souza,
378 R. A. F.: Substantial convection and precipitation enhancements by ultrafine aerosol particles,
379 *Science*, 359, 411–418, <https://doi.org/10.1126/science.aan8461>, 2018.
- 380 Fernald, F. G.: Analysis of atmospheric lidar observations: some comments, *Appl. Opt.*, 23,
381 652–653, <https://doi.org/10.1364/AO.23.000652>, 1984.
- 382 Findeisen, W.: Kolloid-meteorologische Vorgänge bei Niederschlagsbildung, *Meteorol. Z.*, 55,
383 121–133, 1938.
- 384 Garrett, T. J. and Zhao, C. F.: Increased Arctic cloud longwave emissivity associated with
385 pollution from mid-latitudes, *Nature*, 440, 787–789, <https://doi.org/10.1038/nature04636>,
386 2006.
- 387 Giorgi, F., Bi, X. Q., and Qian, Y.: Direct radiative forcing and regional climatic effects of
388 anthropogenic aerosols over East Asia: a regional coupled climate-chemistry/aerosol model
389 study, *J. Geophys. Res.*, 107, 4439, <https://doi.org/10.1029/2001JD001066>, 2002.
- 390 Guo, J. P., Deng, M. J., Lee, S. S., Wang, F., Li, Z. Q., Zhai, P. M., Liu, H., Lv, W. T., Yao, W.,
391 and Li, X. W.: Delaying precipitation and lightning by air pollution over the Pearl River
392 Delta. Part I: observational analyses, *J. Geophys. Res. Atmos.*, 121, 6472–6488,
393 <https://doi.org/10.1002/2015JD023257>, 2016.
- 394 He, H., Gao, Q., Liu, X. E., Zhou, W., and Jia, X. C.: Numerical simulation of the structural
395 characteristics and precipitation mechanism of stratiform clouds with embedded convections,
396 *Chin. J. Atmos. Sci.*, 39, 315–328, <https://doi.org/10.3878/j.issn.1006-9895.1404.14102>,



- 397 2015.
- 398 Heymsfield, A. J., Schmitt, C., Chen, C.-C.-J., Bansemer, A., Gettelman, A., Field, P. R., and
399 Liu, C. T.: Contributions of the liquid and ice phases to global surface precipitation:
400 observations and global climate modeling, *J. Atmos. Sci.*, 77, 2629–2648,
401 <https://doi.org/10.1175/JAS-D-19-0352.1>, 2020.
- 402 Hindman, E. E. and Upadhyay, B. P.: Air pollution transport in the Himalayas of Nepal and
403 Tibet during the 1995–1996 dry season, *Atmos. Environ.*, 36, 727–739,
404 [https://doi.org/10.1016/S1352-2310\(01\)00495-2](https://doi.org/10.1016/S1352-2310(01)00495-2), 2002.
- 405 Hosler, C. L., Jensen, D. C., and Goldshlak, L.: On the aggregation of ice crystals to form snow,
406 *J. Atmos. Sci.*, 14, 415–420, [https://doi.org/10.1175/1520-0469\(1957\)014<0415:OTAOIC>2.0.CO;2](https://doi.org/10.1175/1520-0469(1957)014<0415:OTAOIC>2.0.CO;2), 1957.
- 408 Hua, S., Liu, Y. Z., Luo, R., Shao, T. B., and Zhu, Q. Z.: Inconsistent aerosol indirect effects
409 on water clouds and ice clouds over the Tibetan Plateau, *Int. J. Climatol.*, 40, 3832–3848,
410 <https://doi.org/10.1002/joc.6430>, 2020.
- 411 Huang, J. P., Minnis, P., Yi, Y. H., Tang, Q., Wang, X., Hu, Y. X., Liu, Z. Y., Ayers, K., Trepte,
412 C., and Winker, D.: Summer dust aerosols detected from CALIPSO over the Tibetan Plateau,
413 *Geophys. Res. Lett.*, 34, L18805, <https://doi.org/10.1029/2007GL029938>, 2007.
- 414 IPCC Climate Change 2013: The Physical Science Basis (eds Boucher, O., D. et al.)
415 (Cambridge Univ. Press, 2014). <https://doi.org/10.1017/CBO9781107415324.016>
- 416 Jiang, J., Zhou, T. J., Qian, Y., Li, C., Song, F. F., Li, H. M., Chen, X. L., Zhang, W. X., and
417 Chen, Z. M.: Precipitation regime changes in High Mountain Asia driven by cleaner air,
418 *Nature*, 623, 544–549, <https://doi.org/10.1038/s41586-023-06619-y>, 2023.
- 419 Kang, S. C., Zhang, Q. G., Qian, Y., Ji, Z. M., Li, C. L., Cong, Z. Y., Zhang, Y. L., Guo, J. M.,
420 Du, W. T., Huang, J., You, Q. L., Panday, A. K., Rupakheti, M., Chen, D. L., Gustafsson, Ö.,
421 Thiemens, M. H., and Qin, D. H.: Linking atmospheric pollution to cryospheric change in
422 the Third Pole region: current progress and future prospects, *Natl. Sci. Rev.*, 6, 796–809,
423 <https://doi.org/10.1093/nsr/nwz031>, 2019.
- 424 Khain, A., Rosenfeld, D., and Pokrovsky, A. A.: Aerosol impact on the dynamics and
425 microphysics of deep convective clouds, *Q. J. Roy. Meteorol. Soc.*, 131, 2639–2663,
426 <https://doi.org/10.1256/qj.04.62>, 2005.
- 427 Lau, K. M., Ramanathan, V., Wu, G. X., Li, Z., Tsay, S. C., Hsu, C., Sikka, R., Holben, B., Lu,
428 D., Tartari, G., Chin, M., Koudelova, P., Chen, H., Ma, Y., Huang, J., Taniguchi, K., and
429 Zhang, R.: The joint aerosol-monsoon experiment: a new challenge for monsoon climate



- 430 research, *Bull. Am. Meteorol. Soc.*, 89, 369–383, <https://doi.org/10.1175/BAMS-89-3-369>,
431 2008.
- 432 Lawrence, M. G.: Asia under a high-level brown cloud, *Nat. Geosci.*, 4, 352–353,
433 <https://doi.org/10.1038/ngeo1166>, 2011.
- 434 Levin, Z. and Cotton, W. R.: *Aerosol Pollution Impact on Precipitation: A Scientific Review*,
435 Springer, <https://doi.org/10.1007/978-1-4020-8690-8>, 2009.
- 436 Levy, R. C., Mattoo, S., Munchak, L. A., Remer, L. A., Sayer, A. M., Patadia, F., and Hsu, N.
437 C.: The collection 6 MODIS aerosol products over land and ocean, *Atmos. Meas. Tech.*, 6,
438 2989–3034, <https://doi.org/10.5194/amt-6-2989-2013>, 2013.
- 439 Li, X. F., Kang, S. C., Sprenger, M., Zhang, Y. L., He, X. B., Zhang, G. S., Tripathee, L., Li, C.
440 L., and Cao, J. J.: Black carbon and mineral dust on two glaciers on the central Tibetan
441 Plateau: sources and implications, *J. Glaciol.*, 66, 1–11, <https://doi.org/10.1017/jog.2019.100>,
442 2020.
- 443 Liu, X. D., Xie, X. N., Yin, Z. Y., Liu, C. H., and Gettelman, A.: A modeling study of the effects
444 of aerosols on clouds and precipitation over East Asia, *Theor. Appl. Climatol.*, 106, 343–354,
445 <https://doi.org/10.1007/s00704-011-0436-6>, 2011.
- 446 Liu, Y. Z., Huang, J. P., Wang, T. H., Li, J. M., Yan, H. R., and He, Y. L.: Aerosol-cloud
447 interactions over the Tibetan Plateau: an overview, *Earth Sci. Rev.*, 234, 104216,
448 <https://doi.org/10.1016/j.earscirev.2022.104216>, 2022.
- 449 Liu, Y. Z., Li, Y. H., Huang, J. P., Zhu, Q. Z., and Wang, S. S.: Attribution of the Tibetan Plateau
450 to northern drought, *Natl. Sci. Rev.*, 7, 489–492, <https://doi.org/10.1093/nsr/nwz191>, 2020a.
- 451 Liu, Y. Z., Sato, Y., Jia, R., Xie, Y. K., Huang, J. P., and Nakajima, T.: Modeling study on the
452 transport of summer dust and anthropogenic aerosols over the Tibetan Plateau, *Atmos. Chem.*
453 *Phys.*, 15, 12581–12594, <https://doi.org/10.5194/acp-15-12581-2015>, 2015.
- 454 Liu, Y. Z., Shao, T. B., Hua, S., Zhu, Q. Z., and Luo, R.: Association of anthropogenic aerosols
455 with subtropical drought in East Asia, *Int. J. Climatol.*, 40, 3500–3513,
456 <https://doi.org/10.1002/joc.6410>, 2020b.
- 457 Liu, Z. Y. and Sugimoto, N.: Simulation study for cloud detection with space lidars by use of
458 analog detection photomultiplier tubes, *Appl. Opt.*, 41, 1750–1759,
459 <https://doi.org/10.1364/AO.41.001750>, 2002.
- 460 Lohmann, U. and Feichter, J.: Global indirect aerosol effects: A review, *Atmos. Chem. Phys.*,
461 5, 715–737, <https://doi.org/10.5194/acp-5-715-2005>, 2005.
- 462 Luo, M., Liu, Y. Z., Zhu, Q. Z., Tang, Y. H., and Alam, K.: Role and mechanisms of black
463 carbon affecting water vapor transport to Tibet, *Remote Sens.*, 12, 231,



- 464 <https://doi.org/10.3390/rs12020231>, 2020.
- 465 Ma, Y. M., Xie, Z. P., Ma, W. Q., Han, C. B., Sun, F. L., Sun, G. H., Liu, L., Lai, Y., Wang, B.
466 B., Liu, X., Zhao, W. Q., Ma, W. Y., Wang, F. F., Sun, L. J., Ma, B., Han, Y. Z., Wang, Z. Y.,
467 and Xi, Z. H.: QOMS: a comprehensive observation station for climate change research on
468 the top of Earth, *Bull. Am. Meteorol. Soc.*, 104, E563-E584, <https://doi.org/10.1175/BAMS->
469 [D-22-0084.1](https://doi.org/10.1175/BAMS-D-22-0084.1), 2023.
- 470 Menon, S., Hansen, J., Nazarenko, L., and Luo, Y.: Climate effects of black carbon aerosols in
471 China and India, *Science*, 297, 2250–2253, <https://doi.org/10.1126/science.1075159>, 2002.
- 472 Ming, J., Xiao, C. D., Du, Z. C., and Yang, X. G.: An overview of black carbon deposition in
473 High Asia glaciers and its impacts on radiation balance, *Adv. Water Resour.*, 55, 80-87,
474 <https://doi.org/10.1016/j.advwatres.2012.05.015>, 2013.
- 475 Miao, Q. J., Xu, X. D., and Zhang X. J.: Characteristics of teleconnection wave train for
476 circulation pattern of flood/drought in the middle and lower reaches of yangtze river and sea
477 surface temperature over equatorial eastern pacific. *Acta Meteorol. Sin.*, 60: 688-697.
478 <https://doi.org/10.1016/10.11676/qxxb2002.082>, 2002 (In Chinese).
- 479 Penner, J. E., Hegg, D., and Leaitch, R.: Unraveling the role of aerosols in climate change,
480 *Environ. Sci. Technol.*, 35, 332A–340A, <https://doi.org/10.1021/es0124414>, 2001.
- 481 Purdy, J. C., Austin, G. L., Seed, A. W., and Cluckie, I. D.: Radar evidence of orographic
482 enhancement due to the seeder feeder mechanism, *Meteorol. Appl.*, 12, 199–206,
483 <https://doi.org/10.1017/S1350482705001672>, 2005.
- 484 Qian, Y., Gong, D. Y., Fan, J. W., Leung, L. R., Bennartz, R., Chen, D. L., and Wang, W. G.:
485 Heavy pollution suppresses light rain in China: observations and modeling, *J. Geophys. Res.*,
486 114, D00K02, <https://doi.org/10.1029/2008JD011575>, 2009.
- 487 Ramanathan, V., Chung, C., Kim, D., Bettge, T., Buja, L., Kiehl, J. T., Washington, W. M., Fu,
488 Q., Sikka, D. R., and Wild, M.: Atmospheric brown clouds: Impacts on South Asian climate
489 and hydrological cycle, *Proc. Natl. Acad. Sci. USA*, 102, 5326–5333,
490 <https://doi.org/10.1073/pnas.0500656102>, 2005.
- 491 Ramelli, F., Henneberger, J., David, R. O., Bühl, J., Radenz, M., Seifert, P., Wieder, J., Lauber,
492 A., Pasquier, J. T., Engelmann, R., Mignani, C., Hervo, M., and Lohmann, U.: Microphysical
493 investigation of the seeder and feeder region of an Alpine mixed-phase cloud, *Atmos. Chem.*
494 *Phys.*, 21, 6681–6706, <https://doi.org/10.5194/acp-21-6681-2021>, 2021.
- 495 Rosenfeld, D., Sherwood, S., Wood, R., and Donner, L.: Climate effects of aerosol-cloud
496 interactions, *Science*, 343, 379–380, <https://doi.org/10.1126/science.1247490>, 2014.
- 497 Rosenfeld, D.: Aerosols, clouds, and climate, *Science*, 312, 1323–1324,



- 498 <https://doi.org/10.1126/science.1128972>, 2006.
- 499 Sayer, A. M., Munchak, L. A., Hsu, N. C., Levy, R. C., Bettenhausen, C., and Jeong, M.-J.:
500 MODIS collection 6 aerosol products: comparison between aqua's e-deep blue, dark target,
501 and "merged" data sets, and usage recommendations, *J. Geophys. Res.-Atmos.*, 119, 13965–
502 13989, <https://doi.org/10.1002/2014JD022453>, 2014.
- 503 Tong, Y., Li, J., Jiang, Z. J., Liu, G. Y., Zhang, Z. Y., Zhang, L., Dong, Y. M., and Zhao, C. F.:
504 Increased aerosol scattering contributes to the recent monsoon rainfall decrease over the
505 Gangetic Plain, *Sci. Bull.*, 68, 2629–2638, <https://doi.org/10.1016/j.scib.2023.08.052>, 2023.
- 506 Twomey, S. A., Piepgrass, M., and Wolfe, T. L.: An assessment of the impact of pollution on
507 global cloud albedo, *Tellus B*, 36, 356–366, <https://doi.org/10.3402/tellusb.v36i5.14916>,
508 1984.
- 509 Twomey, S.: The influence of pollution on the shortwave albedo of clouds, *J. Atmos. Sci.*, 34,
510 1149–1152, [https://doi.org/10.1175/1520-0469\(1977\)034<1149:tiopot>2.0.co;2](https://doi.org/10.1175/1520-0469(1977)034<1149:tiopot>2.0.co;2), 1977.
- 511 Wan, B. C., Gao, Z. Q., Chen, F., and Lu, C. G.: Impact of Tibetan Plateau surface heating on
512 persistent extreme precipitation events in southeastern China, *Mon. Weather Rev.*, 145,
513 3485-3505, <https://doi.org/10.1175/MWR-D-17-0061.1>, 2017.
- 514 Wang, C., Wu, C., and Li, L. P.: Data quality analysis and control method of X-band dual
515 polarization radar, *Plateau Meteorology*, 38, 636–649, [https://doi.org/10.7522/j.issn.1000-
516 0534.2018.00096](https://doi.org/10.7522/j.issn.1000-), 2019.
- 517 Wang, T. H., Chen, Y. X., Gan, Z. W., Han, Y., Li, J. M., and Huang, J. P.: Assessment of
518 dominating aerosol properties and their long-term trend in the Pan-Third Pole region: a study
519 with 10-year multi-sensor measurements, *Atmos. Environ.*, 239, 117738,
520 <https://doi.org/10.1016/j.atmosenv.2020.117738>, 2020.
- 521 Wegener, A.: *Thermodynamik der Atmosphäre*, J. A. Barth, Leipzig, 331 pp.,
522 <https://doi.org/10.1038/090031a0>, 1911.
- 523 Xiang, Y., Lv, L. H., Chai, W. X., Zhang, T. S., Liu, J. G., and Liu, W. Q.: Differential phase
524 data quality control of mobile X-band dual-polarimetric Doppler weather radar, *Plateau*
525 *Meteor.*, 31, 223-230, <https://doi.org/10.1088/1748-9326/ab9cfd>, 2012.
- 526 Xiang, Y., Zhang, T. S., Liu, J. G., Wan, X., Loewen, M., Chen, X. T., Kang, S. C., Fu, Y. B.,
527 Lv, L. H., Liu, W. Q., and Cong, Z. Y.: Vertical profile of aerosols in the Himalayas revealed
528 by lidar: new insights into their seasonal/diurnal patterns, sources, and transport, *Environ.*
529 *Pollut.*, 285, 117686, <https://doi.org/10.1016/j.envpol.2021.117686>, 2021.
- 530 Xiao, Y. J., Wang, B., Chen, X. H., Cao, J. W., and Yang, X. M.: Differential Phase Data Quality
531 Control of Mobile X-Band Dual-Polarimetric Doppler Weather Radar, *Plateau Meteorology*,



- 532 31, 223–230, 2012.
- 533 Xu, X. D. and Chen, L. S.: Advances of the Study on Tibetan Plateau Experiment of
534 Atmospheric Sciences, *J. Appl. Meteor. Sci.*, 17, 756–772, 2006 (In Chinese).
- 535 Xu, X. D., Cai, W. Y., Zhao, T. L., Zhang, H., Guo, X. L., Liu, W. Q., Zhang, T. S., Zhao, R. Z.,
536 Wu, C., Li, Y. Q., Wang, L., Yan, P., and Yang, C. J.: Understanding clouds and precipitation
537 over the Mount Qomolangma: how does the aerosol activation effect exist?, *Sci. Bull.*, 70,
538 3649–3658, <https://doi.org/10.1016/j.scib.2025.09.031>, 2025.
- 539 Xu, X. D., Tao, S. Y., Wang, J. Z., Chen, L. S., Zhou, L., and Wang, X. R.: The relationship
540 between water vapor transport features of Tibetan plateau-monsoon “large triangle” affecting
541 region and drought-flood abnormality of China, *Acta Meteorol. Sin.*, 60, 257–266,
542 <https://doi.org/10.11676/qxxb2002.032>, 2002.
- 543 Xu, X. D., Zhou, M. Y., Chen, J. Y., Bian, L. G., Zhang, G. Z., Liu, H. Z., Li, S. M., Zhang, H.
544 S., Zhao, Y. J., Suolongduoji, and Wang, J. Z.: A comprehensive physical image of land-air
545 dynamic and thermal structure on the Tibetan plateau, *Sci. China Ser. D*, 31, 428–440,
546 <https://doi.org/10.1360/zd2001-31-5-428>, 2001.
- 547 Zhang, H., Wang, Z. L., and Zhao, S. Y.: In atmospheric aerosol and its climate effect (1st ed.,
548 In Chinese), China Meteorological Press, Beijing, 2017.
- 549 Zhao, C. F., Li, J. F., and Yang, Y. K.: A short review of microphysical effects of aerosols on
550 clouds and precipitation, *Chin. J. Atmos. Sci.*, 49, 949–963,
551 <https://doi.org/10.3878/j.issn.1006-9895.2503.25015>, 2025.
- 552 Zhao, C. F., Sun, Y., Yang, J., Li, J. F., Zhou, Y., Yang, Y. K., Fan, H., and Zhao, X.:
553 Observational evidence and mechanisms of aerosol effects on precipitation, *Sci. Bull.*, 69,
554 1569–1580, <https://doi.org/10.1016/j.scib.2024.03.014>, 2024.
- 555 Zhao, C. F., Yang, Y. K., Fan, H., Huang, J. P., Fu, Y. F., Zhang, X. Y., Kang, S. C., Cong, Z.
556 Y., Letu, H., and Menenti, M.: Aerosol characteristics and impacts on weather and climate
557 over the Tibetan Plateau, *Natl. Sci. Rev.*, 7, 492–495, <https://doi.org/10.1093/nsr/nwz184>,
558 2020.
- 559 Zhou, X., Bei, N. F., Liu, H. L., Cao, J. J., Xing, L., Lei, W. F., Molina, L. T., and Li, G. H.:
560 Aerosol effects on the development of cumulus clouds over the Tibetan Plateau, *Atmos.*
561 *Chem. Phys.*, 17, 7423–7434, <https://doi.org/10.5194/acp-17-7423-2017>, 2017.
- 562 Zhuo, G., Xu, X. D., and Chen, L. S.: Instability of eastward movement and development of
563 convective cloud clusters over Tibetan Plateau, *J. Appl. Meteor. Sci.*, 13, 447–456, 2002.